

Quantum size effects in the low temperature layer-by-layer growth of Pb on Ge(001)

L. Floreano ^{a,*} D. Cvetko ^{a,b} F. Bruno ^{a,c} G. Bavdek ^{a,b}
A. Cossaro ^a R. Gotter ^a A. Verdini ^a A. Morgante ^{a,c}

^a*Laboratorio TASC-INFM, Basovizza SS-14 Km. 163.5, I-34012, Trieste, Italy.*

^b*also at: J.Stefan Institute, Physics department, University of Ljubljana, Slovenia.*

^c*also at: Physics department, University of Trieste, Italy.*

Abstract

The electronic properties of thin metallic films deviate from the corresponding bulk ones when the film thickness is comparable with the wavelength of the electrons at the Fermi level. This phenomenon, referred to as quantum size effect (QSE), is also expected to affect the film morphology and structure leading to the “electronic growth” of metals on semiconductors. Such effect may be observed when metals are grown on substrates held at low temperature and are manifested through the occurrence of “magical” thickness islands or critical thickness for layer-by-layer growth. In particular, layer-by-layer growth of Pb(111) films has been reported for deposition on Ge(001) below ~ 130 K. An extremely flat morphology is preserved throughout deposition from four up to a dozen of monolayers. These flat films are shown to be metastable and to reorganize into large clusters uncovering the first Pb layer pseudomorphic to the underlying Ge(001) substrate already at room temperature. Indications of QSE induced structural variations of the growing films have been reported for Pb growth on both Si(111) and Ge(001). In the latter case, the apparent height of the Pb(111) monatomic step was shown to change in an oscillatory fashion by He atom scattering (HAS) during layer-by-layer growth at low temperature. The extent of the structural QSE has been obtained by a comparison of the HAS data with X-ray diffraction (XRD) and reflectivity experiments. Whereas step height variations as large as 20% have been measured by HAS reflectivity, the displacement of the atomic planes from their bulk position, as measured by XRD, has been found to mainly affect the topmost Pb layer, but with a lower extent, i.e. the QSE observed by HAS are mainly due to a perpendicular displacement of the topmost layer charge density. The effect of the variable surface relaxation on the surface vibration has been studied from the acoustic dispersion of the low energy phonons, as measured by inelastic HAS.

Key words: He atom-solid scattering and diffraction - elastic and inelastic; X-ray scattering, diffraction and reflection; Epitaxy; Growth, Surface electronic

In the field of surface science, a strong experimental and theoretical effort has been traditionally devoted to the study of the growth and diffusion processes for their relevance in the fabrication of novel electronic devices. From an experimental point of view, the main issue has been to achieve the conditions for layer-by-layer growth or a regular patterning of the growing film in order to obtain sharp interfaces between different materials. In particular much attention has been drawn to a few key cases of the homoepitaxial growth (such as reentrant layer-by-layer growth, inverse growth, ion assisted growth) as well as heteroepitaxial growth (particularly surfactant assisted growth) giving rise to a consistent thermodynamical frame for describing the growth and diffusion processes [1].

While in the past most of the attention was dedicated to high temperature film growth of semiconductors (to fabricate electronic devices), at present the deposition of metals at low substrate temperature is the most attractive field for investigating the correlation between the structural and electronic properties of the film. In heteroepitaxial films, the suppression of thermally activated processes, such as surface diffusion and intermixing, enables the formation of two-dimensional (2D) metal films with sharp interfaces. Thus, the interplay between the structural and electronic lengthscales of the metallic film can be put in evidence. In addition, low temperature growth of metal on metal surfaces is also increasingly employed in the study of magnetic systems thanks to the possibility of inhibiting intermixing processes.

Typically, electronic effects are not observed upon deposition on semiconductors or insulators at room temperature (RT). In fact, most metals display a cluster growth behavior, either in a Wolmer-Weber, or in a Stranski-Krastanov mode. The thermal energy at the metal/semiconductor interface is usually high enough to allow metal adatoms to migrate uphill at the island step edges, thus to explore various thermodynamical configurations. Both the tendency to reduce the interface area and that to reduce the ratio between the cluster area and its volume may favor the formation of three-dimensional (3D) metal clusters. Any electronic effect due to size confinement is then smeared out by the inhomogeneous spatial and size distribution of the clusters. A possible path for growing films with a smoother morphology is to inhibit the uphill flow of the deposited atoms by lowering the substrate temperature. This route has been shown to allow a certain degree of control in the morphology of the growing films leading to the formation of regular patterns of islands with ho-

* Tel: +39 040 3756442, +39 040 3758369; fax: +39 040 226767
Email address: floreano@tasc.infm.it (L. Floreano).

mogeneous size and shape, or even to layer-by-layer growth. Such controlled non-equilibrium morphology can display the effects originated by the quantum confinement of the metal electrons. These phenomena, referred to as quantum size effect (QSE), are clearly manifested by the appearance of quantum well states (QWS) in thin metal films and nanoislands [2,3,4], as well as by the spin density waves observed in heterogeneous magnetic systems [5], which give rise to the exchange magnetic coupling in layered systems [6,7,8]. QSE were first observed by Jaklevic and coworkers, who measured the tunnelling current of thin Pb electrodes [9], while the QWS were directly observed by valence band photoemission from single layer metal films [10]. Later on, QWS have been measured by photoemission in several metal films on both metal [11,12] and semiconductor substrates [13,14,15].

In general, when the thickness D of a metal film is comparable with the Fermi wavelength λ_F of the film electron gas, cyclic variations of the surface charge density and work function are expected as the film thickness approaches an odd multiple of $\lambda_F/4$ [16]. As new layers are added to the metal film, cyclic variations of the perpendicular displacement of the surface charge density should be observed. Among different metals, Pb is certainly a suitable candidate to display strong QSEs, since its bulk interlayer spacing $d_{Pb} = 2.86 \text{ \AA}$, along its preferred growth orientation [111], is $\sim \frac{3}{4}\lambda_F$ [17]. Deviations of the physical properties in thin Pb films from the bulk ones are thus expected with a bi-layer periodicity.

The first evidence of such oscillatory behavior dates back to the works by Jalochofski and Bauer, who measured the electrical resistivity [18,19], valence band photoemission [20] and the RHEED reflectivity [18,21] during Pb deposition on Si(111)-(7 \times 7) and Si(111)-Au(6 \times 6) at low temperature. Double layer modulations, characteristic of QSE, were observed in both resistivity and RHEED, with their amplitude increasing with the quality of the growing film surface (domain size and flatness). Unexpectedly, the best growth conditions were achieved at the lowest temperatures down to 16 K. In this temperature range, no kinetic mechanisms are activated and other mechanisms must be involved in the diffusion process. In fact, it was also observed that variations of the growth rate by a factor of 20 were yielding the same shape of the RHEED oscillations, i.e. the same film morphology [21]. The same system was later studied by X-ray diffraction (XRD) and compared to He atom scattering (HAS) and RHEED reflectivity [22,23]. Interestingly, Hibma and coworkers found that the crystalline structure of Pb(111) is only observed after the deposition of 5 ML of Pb [23], the same thickness also corresponds to the onset of an almost layer-by-layer growth [22].

The existence of a critical thickness for the formation of a flat surface appears to be characteristic of the low temperature growth of metal on semiconductors, having been also observed for Pb on Ge(001) with HAS [24] and for Ag on

Si(111) [25], GaAs(110) [26,27], and other III-V compounds [28] with STM. Below the critical thickness or at intermediate substrate temperature, the metal clusters have been found to display a regular prismoidal shape with a flat surface. These flat islands display a preferred thickness, i.e. only bi-layer islands are observed for Ag on Si(111) [29], while odd n -layer islands ($n = 5, 7, 9$) are favored for Pb on Si(111) [30,31,32]. In the latter case, Tringides and coworkers demonstrated the possibility to grow Pb islands with homogeneous thickness by properly selecting the substrate temperature and Pb coverage [32], or even by changing the substrate reconstruction upon pre-deposition [31,33].

The stability of these flat morphologies has been recently discussed on the basis of a detailed balance among the energetics of the charge quantum confinement, the charge transfer at the interface, the Friedel's charge density oscillation and the stress at the interface [34,35]. These competing phenomena can lead to the manifestation of the "electronic growth" of metals on semiconductors, i.e. to the existence of a critical thickness for the onset of layer-by-layer growth and/or magic islands.

These flat "magic" islands represent an almost ideal quantum box for the metal Fermi electrons and QSE can be observed by means of a local probe such as STM. Altfeder measured by STM the electron interference fringes on the flat surface of a Pb quantum wedge grown on a staircase of Si(111) terraces [36]. In a similar fashion, an oscillatory variation of the monatomic step height as a function of the film thickness was observed in Pb layer-by-layer growth on a flat Ge(001) surface by He atom reflectivity, i.e. by a probe sensitive only to the surface charge density [24]. The apparent step height was found to oscillate around the value of the Pb(111) bulk interlayer spacing with an amplitude up to 20%. According to theoretical calculations, these variations should be accompanied by the relaxation of the topmost film layer, so that the structural variations of the film partly counteract the extent of the electronic property variations [37]. More detailed calculations indicate that all the interlayer spacings of the growing film should be affected by QSE [38,39], in such a way to further minimize the total energy. In fact, indirect evidence of a structural effect has been recently found by Tsong via STM spectroscopy on Pb magic islands, where the deviation of the apparent step height, has been studied as a function of the tip bias voltage. Furthermore, the energy separation between the highest filled states and the lowest empty ones has been studied as a function of the island thickness to assign the quantum number to the QWS within the islands [40].

In the following section, the low temperature deposition of Pb on Ge(001) is characterized by both HAS and X-ray reflectivity (XRR) measurements. The existence of a critical thickness for the formation of crystalline Pb(111) islands as well as for the onset of layer-by-layer growth is discussed. An ex-

tremely flat morphology is observed throughout deposition from five up to a dozen of monolayers, then the number of exposed layers starts to increase. These flat films are shown to be metastable and to reorganize into large clusters uncovering the first Pb layer pseudomorphic to the underlying Ge(001) substrate upon annealing to room temperature.

A direct measurement by X-ray diffraction of the topmost layer relaxation and inner layer spacing distribution is presented in the thickness range of layer-by-layer growth. These results are compared with previous values of the monatomic step height measured by HAS. Whereas step height variations up to 20% have been measured by HAS reflectivity, the displacement of the atomic planes from their bulk position, as measured by X-ray diffraction (XRD), is found to mainly affect the topmost Pb layer, but with a much lower extent, i.e. the QSE observed by HAS are mainly due to a perpendicular displacement of the topmost layer charge density. Finally, we will present the effect of the oscillating surface relaxation on the surface phonons of the Pb(111) film surface, as measured by the inelastic HAS.

1 Experimental

The experiments have been performed with the HAS apparatus of the I.N.F.M.-TASC National Laboratory [41] and at the Elettra Synchrotron facility in Trieste (Italy) with the I.N.F.M. ALOISA beamline [42]. Both experimental stations make use of the same type of manipulator (a 6-degree of freedom manipulator with 0.01° precision on each rotation axis), sample holder, MBE cryo-panel and sputter gun, thus allowing us to easily exchange the samples between the two systems and to adopt the same preparation procedures. In the ALOISA end station, X-ray photoemission is used to check for the substrate cleanness and a RHEED system is used to check for the surface long range order prior to Pb deposition. The experiments have been performed on a set of about a dozen of different Ge(001) samples obtained by different wafers and rods. The substrate is cleaned by Ar^+ ion bombardment at 1 keV, while annealing the sample up to about 1000 K ($T_m = 1211$ K) and monitoring the half-integer peaks of the (2×1) reconstruction. Both heating and sputtering are switched off at the occurrence of the $(2 \times 1) \rightarrow (1 \times 1)$ phase transition. Upon cooling below ~ 240 K, this procedure yields a well ordered $c(4 \times 2)$ structure with average domain size of ~ 1000 Å [43]. The $c(4 \times 2)$ symmetry corresponds the ground phase of the Ge(001) surface and it was shown to be formed by buckled Ge dimers (tilt $\sim 19^\circ$) with an alternate arrangement of the buckling angle orientation [44]. This phase, mimicking an antiferromagnetic ordering of the dimers, undergoes an order-disorder 2D-Ising transition to a (2×1) phase at 240 K, thus locally preserving the same structure of the low temperature (LT) phase [43].

Pb is evaporated from both commercial (EPI) and home-made Knudsen cells with boron nitride crucibles at a temperature of about 800 K. The deposition is monitored in real time either by He reflectivity or by X-ray reflectivity, at the same time quartz microbalances are used to normalize the deposition rate.

In the 110° fixed scattering geometry of our HAS apparatus, the perpendicular He momentum transfer is $K_{He}^\perp = 2K_{He} \cos 55^\circ$, where the He wavevector K_{He} can be varied between 6 and 12 \AA^{-1} by controlling the temperature of the nozzle source. Pb deposition was monitored by He reflectivity at fixed He wavevector. The step height on the growing surface was determined by measuring the He reflectivity as a function of the He wavevector after stopping deposition at a given stage. In fact, almost no kinetic evolution (recovery) was observed at the considered temperature. For a stepped surface this measurement gives rise to reflectivity maxima and minima due to the interference between the He waves scattered by terraces of different height. A rough estimate of the step height can be obtained by the oscillation period, when only two layers are exposed on the surface [45].

The X-ray diffraction and reflectivity measurements have been taken at the end station of the ALOISA beamline. X-ray reflectivity has been measured at a fixed grazing angle of $\alpha = 8.25^\circ$ and for a few photon energies. In this case, maxima and minima of the reflectivity arise from the interference between the X-ray wave reflected by the film/substrate interface and that reflected by the film surface. The period of the reflectivity oscillation yields the film thickness corresponding to the selected perpendicular momentum transfer $K^\perp = 2K \sin \alpha$. Measurements have been performed in a photon energy range from 5 up to 6.5 keV, corresponding to periodic interference conditions from film thickness ranging from $\Delta D = 8.64$ to 6.58 \AA , respectively, i.e. from 3 to 2.3 ML, in units of Pb(111) bulk interlayer spacings. X-ray reflectivity thus measures the overall film thickness as opposed to He scattering, which only probes the terrace distribution of the exposed surface layers. For a few selected deposition stages in proximity of the critical thickness for the onset of layer-by-layer growth, the deposition has been stopped and scans with the perpendicular momentum transfer have been taken along the $(2, \bar{2}, 0) + L(1, 1, 1)$ rod of the Pb diffraction peak. In this case, maxima and minima are due to the diffraction grating formed by the interlayer spacings of the Pb(111) atomic planes. The perpendicular distribution of the Pb film layers can be obtained by fitting a kinematic scattering model to the rod scans.

2 Low temperature layer-by-layer growth

Pb deposition initially leads to the formation of a few ordered pseudomorphic structures in the submonolayer range [46]. The highest coverage ordered

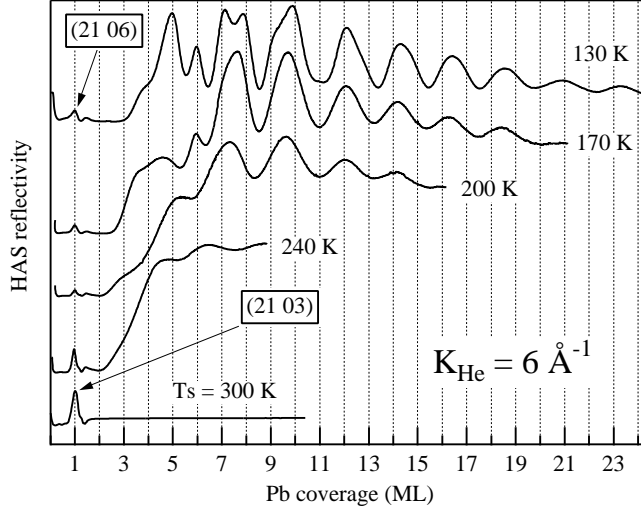


Fig. 1. He specular reflectivity during Pb deposition taken for a few substrate temperatures at He wavevector $K_{He} = 6 \text{ \AA}^{-1}$. The scattering plane has been kept azimuthally oriented along the direction of the main Pb(111) symmetry axis, i.e. at 45° from the substrate [001] direction.

structure displays a (21 03) symmetry reconstruction [which undergoes a transition to a (21 06) symmetry phase at LT] and corresponds to the deposition of about one monolayer (ML) of Pb(111), that is about $5/3$ ML in units of the Ge(001) atom density [47]. The addition of just a few percent of Pb leads to a mixed phase of coexisting (21 03) and $c(4 \times 8)$ -incommensurate domains [48]. Upon further deposition at room temperature (RT) large and widely spaced 3D clusters are formed which do not yield a coherent contribution to He scattering, thus almost not affecting the He reflectivity. It was previously shown that, at low temperature, irregular He reflectivity oscillations can be detected with an amplitude increasing as the temperature is decreased. The deposition curves for a few substrate temperatures are shown in Fig. 1. Layer-by-layer growth conditions are met for substrate temperatures lower than $\sim 130\text{--}140$ K in the $4 - 12$ ML thickness range.[24] The irregular shape of the oscillations is strongly dependent on the selected He wavevector and it is always perfectly reproducible.

A set of He reflectivity curves taken at different He wavevectors is shown in Fig. 2 for deposition on the substrate held at $T_s = 120 - 130$ K. All the reflectivity curves have been normalized to a constant deposition rate by quartz microbalance measurements. The deposition rate has been calibrated a posteriori by a detailed analysis of the reflectivity as a function of the perpendicular momentum transfer K_{He}^\perp for each deposition stage (see left panel in Fig. 3) [49]. The corresponding oscillation of the (0,0) peak width and intensity yields the height of the terrace step [45]. Due to the high interference order, the step height can be accurately determined by the positions of maxima and min-

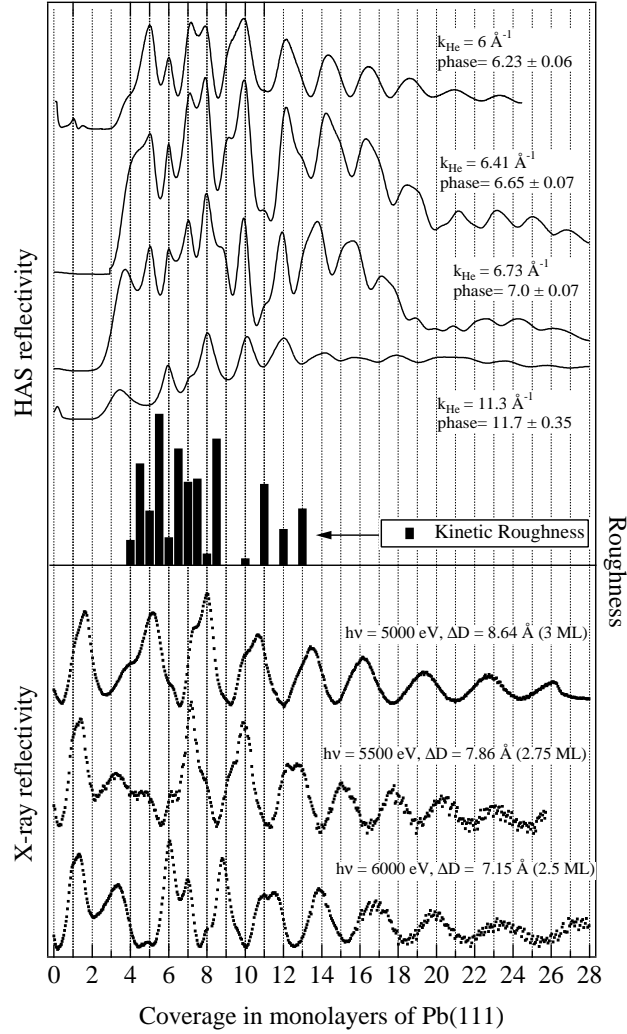


Fig. 2. Top: He reflectivity curves (full line) taken during deposition at $T_s = 130 \text{ K}$ for four He wavevectors, as indicated by the corresponding labels. The scattering plane has been kept azimuthally oriented along the ΓM direction of the main Pb(111) symmetry axis, i.e. at 45° from the substrate [001] direction. Middle: the vertical bars (right y axis) represent the kinetic roughness, i.e. the amplitude of the reflectivity oscillations taken as a function of the perpendicular momentum transfer, as shown in the left panel of Fig. 3. Bottom: X-ray reflectivity curves (filled markers) taken at fixed grazing energy for a few photon energies. The same deposition conditions as in the HAS experiments have been used.

ima. At the same time, the amplitude of the oscillations is proportional to the degree of surface roughness (density of steps). In this way, a consecutive sequence of alternating flat and rough surface has been identified in the first 7-8 oscillations (see the right panel in Fig. 3), corresponding to a layer-by-layer regime of growth [24].

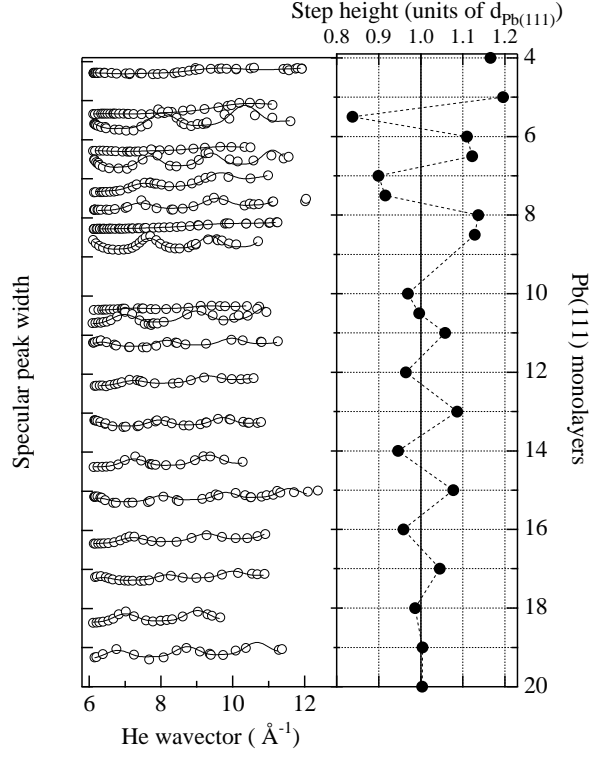


Fig. 3. Left panel: the width of the HAS specular peak (open circles) is taken as a function of the He wavenumber for different Pb coverage. Each curve has been simulated (full fitting line) with a two-level model by using the coverage of the two levels and the step height as fitting parameters. The curves have been vertically shifted by a constant offset proportional to the Pb coverage, which is reported on the right y axis. Right panel: the step height as determined from the analysis of the left panel is reported as a function of the Pb coverage, after Ref. [24]. The step height (horizontal top axis) is reported in units of the Pb(111) interlayer spacing.

Maxima and minima corresponding to the deposition of each new layer are easily detected in the curves of Fig. 2. Interestingly, the roughness minima detected in the layer-by-layer regime, which correspond to extremely flat surfaces, occur at the completion of even-layers deposition, i.e. at 4, 6, 8 and 10 ML. Less flat surfaces are observed in correspondence with odd-layers completion, thus indicating that Pb films of even number of (111) Pb layers are energetically more stable. Interestingly, Tringides et al. found that the most favored Pb islands on Si(111) have odd-layer heights (5, 7 and 9) [31,32,33]. However their Pb island heights were measured by LEED and STM relatively to the pseudomorphic layer [32] and not to the substrate surface, as in the present case.

The highest sensitivity to the surface roughness is obtained at $K_{\text{He}} = 6.73 \text{ \AA}^{-1}$, which corresponds exactly to an out-of-phase scattering condition for the Pb(111) bulk interlayer spacing. Only the flattest stages yield intensity max-

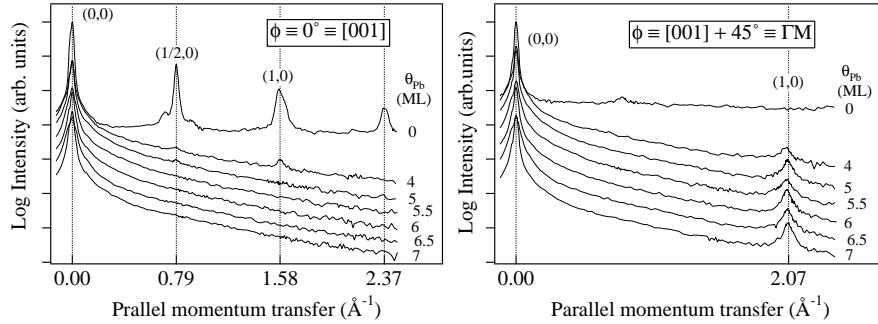


Fig. 4. Left panel: He diffraction scans taken along the $[001]$ direction of Ge for different coverage of Pb. The half-integer peaks of the clean $c(4 \times 2)$ Ge(001) surface are also present in the mixed $(21 \times 06) + c(4 \times 8) - i$ phase. Right panel: He diffraction scans taken along the ΓM Pb(111) direction, i.e. at an azimuthal angle $\phi = 45^\circ$ from the $[001]$ direction of Ge, for the same Pb coverage of the left panel. The diffraction peaks of the Pb(111) surface are only observed.

ima at $K_{He} = 11.3 \text{ \AA}^{-1}$, partly for its close in-phase scattering condition, mostly because of the larger spread in the He wavevector at this energy, which smears the interference among the He waves scattered by different terraces. In this case, the oscillations mainly display a bi-layer periodicity. Interestingly, also the other curves display a bi-layer modulation of the layer-by-layer oscillations, which evolves towards bi-layer oscillations beyond 10-12 ML. We observed a similar behavior also for the LT deposition of Pb on Ge(111), where the main difference appears to be that lower substrate temperatures are required to have a complete substrate wetting [50]. Double layer growth was also observed by HAS to be favored at certain thickness for LT deposition of Pb on Cu(111) [51] and a bi-layer periodicity of the HAS reflectivity was observed for Pb on Cu(100) [52] and Si(111) [22]. According to the energy balance model of Zhenyu Zhang, this bi-layer periodicity is due to the Friedel's oscillation of the Pb electron density in a semi-infinite slab. In fact, consecutive layers correspond to alternating maxima and minima of the electron density perpendicular profile, the minima favoring the stabilization of a flat surface [34].

2.1 Wetting of the low temperature film

It must be pointed out that, in order to observe the interference effect between the growing layers, Pb growth must proceed coherently over a large surface area, since HAS scattering is averaged over an effective illuminated area of about 0.5 mm^2 . In the early stage of deposition, growth seems to proceed via random nucleation of 3D Pb clusters and the HAS diffraction peaks of the Pb(111) surface are first observed at about 4 ML. The Pb(111) surface is incommensurate with the substrate and its main symmetry axis ΓM is found to be oriented at 45° with respect to the $[001]$ substrate direction. In fact, two

Pb(111) domains rotated by 90° are found, which is the only fingerprint left from the substrate squared lattice.

HAS diffraction from a Pb(111) surface first appears at $\theta = 4$ ML. At this coverage, the Pb film is not yet wetting the whole substrate, in fact the diffraction peaks originated by the substrate pseudomorphic structure are still detected (see left panel of Fig. 4). This could be due either to fragmentation of the film into flat islands, as commonly observed for Pb on Si(111) [31,40], or to the occurrence of deep pits uncovering the substrate, as observed for Ag on Si(111) and GaAs(110) [25,26]. However, just after the deposition of one additional layer, the substrate peaks disappear and the Pb(1,0) peaks reach their nominal position [53] without any further shift as the thickness increases, i.e. no lateral strain is observed beyond 5 ML. At this coverage, we cannot exclude the occurrence of small pits, which would be hidden due to shadowing effects. At 5 ML of Pb, the pits uncovering the pseudomorphic Pb layer would be 4-layer deep and their maximum lateral size for not being detected would be 3 nm, to be compared with an average domain size of 13 nm (calculated from the Pb(111) peak width) or an average terrace size of 25 nm (calculated from the specular peak width).

X-ray reflectivity measurements, shown in the bottom of Fig. 2, also support the model in which a flat surface is formed at the completion of the 5th Pb monolayer. The X-ray reflectivity oscillations have a thickness periodicity corresponding to the selected momentum transfer, but, in case of a perfect layer-by-layer growth, cusp-like features are superimposed to the oscillations, due to an overall increase of the reflectivity whenever a flat surface is formed [54]. We have fitted the X-ray reflectivity to a simple growth model with the scattered intensity calculated as:

$$I(t) = \left| F_{Ge} + \sum_1^n \theta_n(t) \cdot f_{Pb} \cdot \rho_{Pb} \cdot e^{iK^\perp z_n} \right|^2; \quad (1)$$

where F_{Ge} and f_{Pb} are the Ge substrate structure factor [44] and Pb atomic scattering factor [55], respectively, ρ_{Pb} is the atom density of a Pb(111) layer, z_n is the perpendicular coordinate of the n -layer and $\theta_n(t)$ is the instantaneous coverage of the n -layer. The layer filling as been described according to a conventional birth-death model [56]:

$$\frac{d\theta_n}{dt} = (1 - \eta_{n-1}) \frac{R}{\rho_{Pb}} (\theta_{n-1} - \theta_n) + \eta_n \frac{R}{\rho_{Pb}} (\theta_n - \theta_{n+1}); \quad (2)$$

where R is the deposition rate (in atom per second and unit area) and the interlayer diffusion probability η_n is a phenomenological effective parameter describing both the intra- and inter-layer atom diffusion [57]. All the interlayer

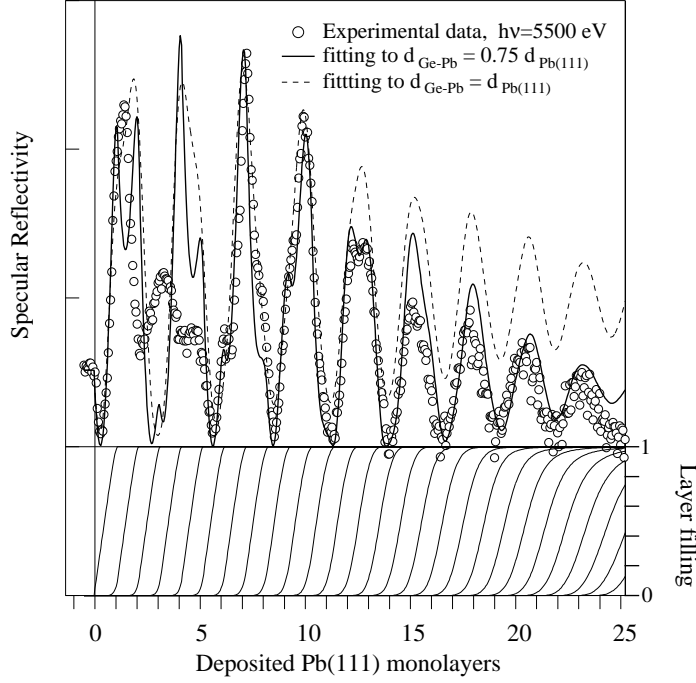


Fig. 5. Top: the X-ray reflectivity taken at 5500 eV during Pb deposition at 130 K (open circles) is simulated by a birth-death growth model. Layer-by-layer growth is established from the 5th Pb ML. The best fit yields a contracted interface thickness (full line), whereas the average intensity of the reflectivity is overestimated when using the unrelaxed Pb(111) spacing for the interface width (dashed curve). Bottom: the single layer filling is reported on the right axis.

Pb(111) spacings have been kept fixed to the bulk value, while the separation $d_{\text{Pb-Ge}}$ between the first (bottom) Pb layer and the substrate has been fitted to obtain the interface thickness. This parameter strongly affects the average reflectivity intensity, which is asymptotically matched at high coverage.

As can be seen in Fig. 5, a contracted interface thickness has been found corresponding to $d_{\text{Pb-Ge}} = 0.75 d_{\text{Pb(111)}}$. From Fig. 5, it can be seen that the first cusp-like feature, corresponding to a flat surface, is found after the deposition of 5 ML, a similar feature is observed at any photon energy (compare with X-ray reflectivities shown in Fig. 2). At lower coverage, the experimental data show similar oscillations for all the considered perpendicular momentum transfer, which cannot be reproduced by any layer-by-layer growth simulation. From comparison with HAS reflectivity, we can say that in this coverage range the Pb film is growing with 3D islands, which are also undergoing a morphological transformation towards an homogeneous flat film of 5 ML.

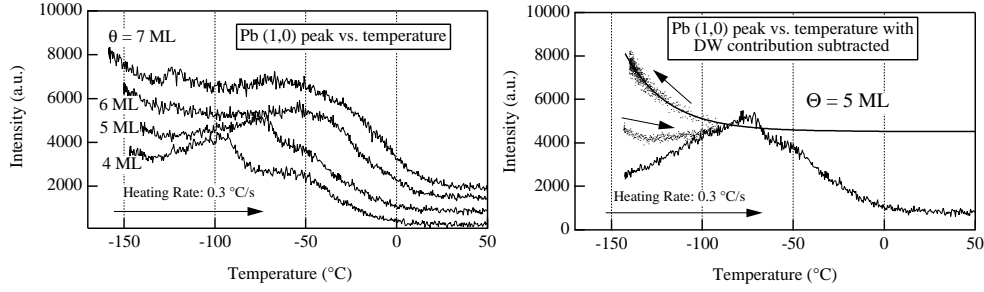


Fig. 6. Left panel: the (1,0) He diffracted intensity of the Pb(111) sample is shown as a function of the temperature at a constant annealing rate. Four scans are shown, corresponding to the measurements taken on Pb films of different coverage. The diffraction from the Pb(111) surface irreversibly disappears above $\sim -50^\circ\text{C}$. Right panel: by annealing below the deconstruction temperature (dotted curve, arrow pointing right) the Pb(111) surface quality (domain size) is increased as witnessed by the strong intensity increase obtained upon cooling down (dotted curve, arrow pointing left). The Debye-Waller exponential attenuation (full line) on the given Pb film can be obtained from the cooling branch of the temperature ramp. The full heating ramp displayed in the left panel at 5 ML is also shown for comparison after the Debye-Waller attenuation correction.

2.2 Metastability of the low temperature film

The Pb film, grown layer by layer below 130 K, is always found to be kinetically frozen for thickness up to a few dozen monolayers. Whenever the LT Pb film is annealed to the room temperature, the Pb(111) diffractions peaks disappear and only the diffraction from the pseudomorphic phase is detected (both with HAS and X-ray scattering), thus suggesting a fragmentation of the film into large clusters uncovering the Pb/Ge interface.

In fact, the LT smooth and wetting film appears to be metastable, as substrate temperatures lower than 130 K are required for the onset of regular layer-by-layer growth, but the surface quality (terrace and domain size as obtained by the diffracted peak widths) can be increased by short annealing up to 190 K of the Pb film after deposition. The intensity of the Pb(1,0) diffracted peak, shown in Fig. 6, has been taken for a few film thickness during annealing at a constant rate. The Pb(1,0) irreversibly disappears beyond a deconstruction temperature ranging from 190 to 220 K, depending on the film thickness. If the film is annealed below the critical temperature and then cooled down, the Pb(111) domain size can be almost doubled. Further deposition on the annealed film yields reflectivity oscillations with larger amplitude (for both HAS and X-ray reflectivity), i.e. more perfect layer-by-layer growth conditions are met. Similarly, pre-deposition at RT of 1 ML, leading to the formation of a pseudomorphic (21 03) phase with larger domains, yields better layer-by-layer growth upon further deposition at LT.

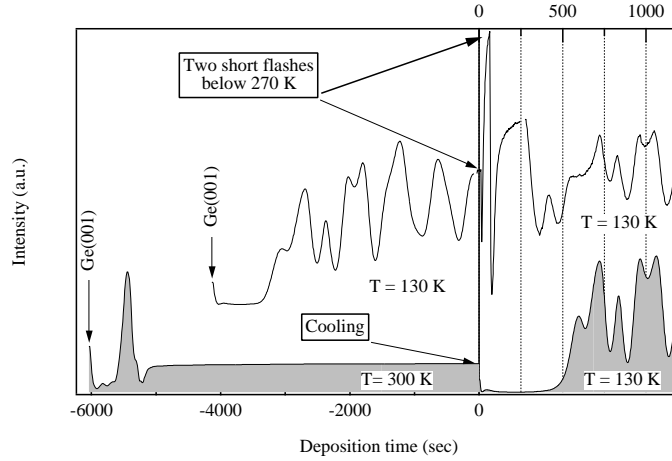


Fig. 7. Upper curve: He reflectivity during Pb deposition up to 13 ML at 130 K, then the Pb shutter is closed ($t=0$). A short flash at 200 K yields a better ordered Pb(111) film. A second flash at 250 K causes the fragmentation of the Pb film. Further deposition ($t=270$) at 130 K yields the layer-by-layer growth features characteristic of the deposition on the clean substrate. Lower curve (shadowed): extended Pb deposition at 300 K does not yield any growth feature after the formation of the pseudomorphic phase at 1 ML. The deposition is stopped and the sample is cooled down to 130 K, then Pb deposition is started again ($t=0$) with the same rate. The typical LT layer-by-layer growth oscillations set in again. All curves have been taken with the same He wavenumber of 6 \AA^{-1} and along the same azimuthal orientation $[001]+45^\circ$.

The fragmentation of the wetting Pb film can be demonstrated by the measurement shown in Fig. 7, where 13 ML of Pb are deposited at LT. First the film is well ordered by a short flash to 200 K, then the decomposition is activated by a flash to 250 K and quickly frozen by a rapid quench to 130 K. Further LT deposition yields the same layer-by-layer growth oscillations, as for original deposition on the clean substrate. We must conclude that Pb growth on existing large 3D islands yields an uncorrelated contribute to the He scattering, while the oscillations are due to coherent growth on the uncovered Pb/Ge interface. The reduced amplitude of the reflectivity oscillations reflects the smaller uncovered area of the substrate, where coherent layer-by-layer growth can take place.

A similar behavior is observed when depositing Pb at RT, where no ordered structure formation is observed after the formation of the pseudomorphic phase at 1 ML, and then cooling down below 130 K to continue the deposition (as shown in Fig. 7): layer-by-layer growth is observed again, as for a clean substrate. The only difference with the reflectivity measurements of Fig. 2 is the time required for the onset of layer-by-layer growth, which is delayed on the pre-deposited substrate. The Pb islands thus act as a sink for the diffusing adatoms, delaying the formation of the flat film.

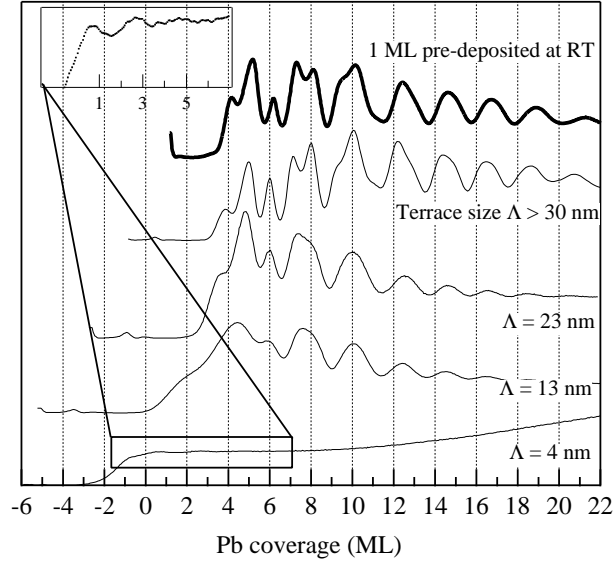


Fig. 8. He reflectivity taken during LT Pb deposition on Ge surfaces with different average terrace size Λ . Each curve is labelled by the corresponding Ge(001) terrace size (in nm). The top curve (thick line) has been obtained by deposition of the 1st Pb ML at RT and further deposition at LT.

The sharpness of the interface seems to play a fundamental role in the onset of layer-by-layer growth. Pb deposition at 130 K has been performed on Ge(001) of different average terrace size, as obtained by controlled ion erosion [58]. As can be seen from Fig. 8, the larger the terrace size is, the larger are the amplitudes of the reflectivity oscillations. As the average terrace size is decreased one observes an increasing delay in the onset of layer-by-layer oscillations and an anticipation of the bi-layer modulation. For the narrower terrace width, only faint double layer modulations are observed, which are superimposed on a rather intense He reflectivity background indicating the formation of a metallic surface.

3 Surface relaxation of the growing film

Concerning the irregular, but reproducible, shape of the HAS layer-by-layer oscillations, a detailed study of the reflectivity as a function of K_{He} found it to be originated by an oscillatory variation of the apparent monatomic step height as new layers are added (see right panel of Fig. 3), i.e. to an oscillatory change of the interference conditions from the Pb(111) terraces [24]. These oscillations have been attributed to QSE, i.e. to perpendicular displacements of the surface charge density occurring whenever new QWS can be accommodated below the Fermi level as the film thickness D_{Pb} is increased. This mechanism has been experimentally confirmed by STM spectroscopy on

individual flat Pb islands grown on Si(111), where the quantum numbers have been assigned to each quantized state for islands of different thickness [40]. It has been shown that adding a new layer increases the number of bound states below the Fermi level by either one or two for islands of consecutive layer thickness (recall that three new bound states can be accommodated for each bi-layer thickness increase, since $d_{Pb} \sim \frac{3}{4}\lambda_F$), which corresponds to a cyclic variation of the energy separation between the Fermi level and the highest occupied state (see left panel of Fig. 9). As a consequence the slope of the in-vacuum tail decay of the total surface charge density $\rho(z)$ is also changing, and the corresponding turning point for He atoms scattered by the surface is perpendicularly displaced in an oscillatory fashion (see right panel of Fig. 9).

In fact, in a critical revision of the HAS study published in Ref. [51], Toennies et al. argued that the apparent oscillations of the step height are to be entirely attributed to the cyclic displacement of the He turning point due to the electronic QSE [59], while ab initio calculations predict the ionic cores to follow the displacement of the charge density, even if to a lower extent [37,38]. On the other hand, the phenomenological model used in Ref. [51] to estimate the in-vacuum charge spillout was supported by ab initio calculation for a Pb(111) slab of up to 15 layers [60]. Slight oscillations of the surface relaxation ($\pm 1\%$) and of the topmost interlayer spacings were predicted as a function of the slab thickness, which did not alter the average -5% compression of the topmost to second layer spacing and the average +2% expansion of the 2nd to 3rd layer spacing. These calculated average values are in good agreement with the experimental ones obtained on a Pb(111) bulk sample [61].

In order to discriminate between the different relaxation models, we used surface X-ray diffraction to measure the perpendicular distribution of the Pb(111) layers within the growing film. For a few selected thicknesses we collected the X-ray data as a function of the perpendicular momentum transfer along the Pb(111) crystal truncation rod, i.e. the diffracted intensity distributed in the reciprocal space among the Bragg reflections. The Pb(111) layer spacings can be determined by fitting the X-ray interference fringes detected along the rod scan. In particular, we measured the $(2, \bar{2}, 0) + L(1, 1, 1)$ rod from the in-plane $(2, \bar{2}, 0)$ peak ($L=0$) up to $L \sim 1.4$, through the out of plane $(3, \bar{1}, 1)$ peak ($L=1$). Each point along the rod scan has been individually fitted in order to obtain the appropriate background subtraction and integrated intensity, as reported in Fig. 10.

First of all, it must be pointed out that the Pb(111) in-plane diffraction peak first appears at a Pb coverage of ~ 2.5 ML, in contrast to the amorphous growth reported for Pb on Si(111), where the XRD peaks of crystalline Pb(111) are first observed after 5 Pb monolayers [23]. At the coverage of 2.5 ML, the diffracted intensity is not high enough for measuring the entire rod scan, however at least three Pb(111) layers can be observed approaching

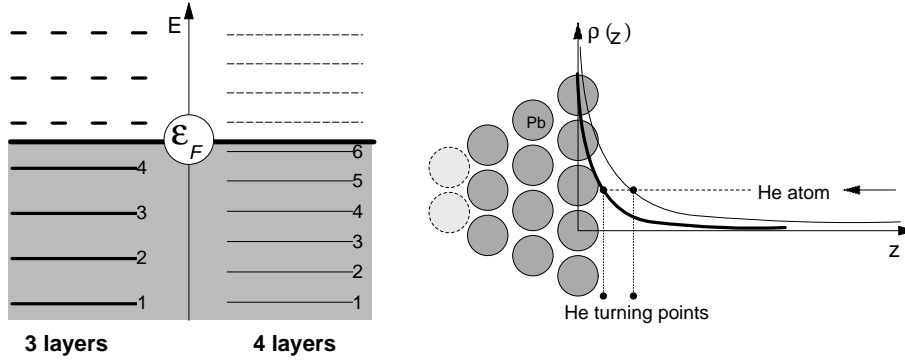


Fig. 9. Left panel: the individual bound states in a 3-layer thick Pb film are indicated with full thick lines at the left-hand side; four states are accommodated below the Fermi level. The thickness increase by one layer allows two new bound states to fall below the Fermi level (thin full lines on the right-hand side). Right panel: the in-vacuum tail decay of the surface charge density $\rho(z)$ is schematically represented for the two cases of the left panel. Thick and thin lines are assigned to the 3- and 4-layer thickness Pb films, respectively. The two iso-density perpendicular coordinates for the He turning point (and for the STM tip distance from the surface) are also shown.

the coverage of 3 ML. Keeping in mind that a large uncovered area of pseudomorphic layer is clearly detected by HAS at this coverage, we can conclude that the X-ray diffraction yield is given by largely spaced 3D islands.

We did not directly measure the structure evolution of the pseudomorphic layer below the growing Pb(111) islands. In fact, the stability of a pseudomorphic phase was observed by X-ray diffraction for Pb on Si(111), where the diffraction peaks from the Pb-induced (7×7) reconstruction were still detected after the deposition of 1800 Å of Pb [62]. However, the same authors found that the $(\sqrt{3} \times \sqrt{3}) - R30^\circ$ Pb-induced reconstruction is destroyed by the growing islands [62]. The different number of metal atoms per unit cell, which are covalently bound to the substrate, probably determines the stability criteria of the pseudomorphic layer. In our case, when entering in the layer-by-layer growth regime, the number of Pb(111) layers is found to be equal to the number of deposited monolayers, thus suggesting the deconstruction of the pseudomorphic layer to be incorporated in the Pb(111) film (recall that the pseudomorphic layer as practically the same atom density of a Pb(111) layer [47]). Both the appearance of the first Pb islands with a three-layer thickness and the onset of layer-by-layer growth at a thickness of five Pb(111) layers qualitatively agree with the magic and critical thickness predicted by the Zhang's model for Pb growth on semiconductors [34]. However, the enhanced surface flatness observed by HAS at even-layer multiples (see the low kinetic roughness at 4, 6, 8, 10 ML in the middle panel of Fig. 2) asks for more refined calculations to understand the role played by the pseudomorphic interface.

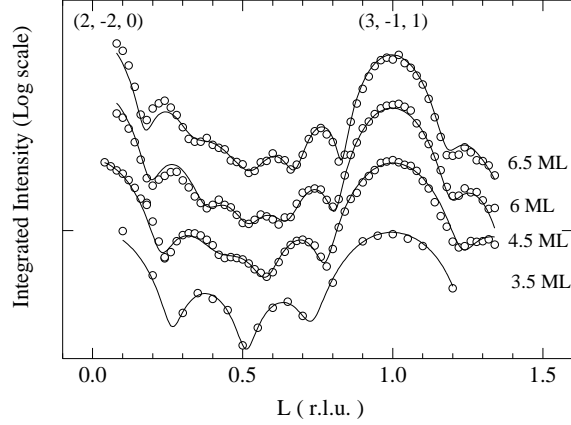


Fig. 10. X-ray diffraction scans of the $(2, \bar{2}, 0) + L(1, 1, 1)$ rod taken after the deposition of 3.5, 4.5, 6 and 6.5 ML of Pb. The experimental data (open circles with error bars) are simulated with a structural model as described in the text (full line).

In a kinematical scattering scheme, the integrated intensities of diffraction peaks are proportional to the modulus square of the crystal structure factors, whose magnitude can be simulated in order to retrieve the atomic plane positions. The rod scan simulations were computed using both home-made routines [63] and the freely distributed ROD program [64], which yielded equivalent results. Since the Pb(111) layers are incommensurate with the substrate and no accidental superposition with the Ge rods occurs, the calculation can be performed for a free standing Pb film. The interlayer spacings, the Debye-Waller attenuation factors and the layer fillings have been used as fitting parameters. For the 6 and 6.5 ML Pb coverage films, we have reduced the total number of fitting parameters (up to 18 could be considered) by considering a complete layer filling except for the topmost layer, as suggested by the HAS and X-ray reflectivity measurements. A good reproduction of the measured curves was possible only by assuming a strong layer-dependence of the Debye-Waller (DW) factors. The DW factor for a bulk Pb crystal is available from the literature as derived from experimentally determined phonon density of states [65]. For a crystal temperature of 130 K, the thermally averaged rms displacement of a bulk atom from its equilibrium position is expected to be $\sqrt{\langle u^2 \rangle} = 0.11 \text{ \AA}$. In general we found larger DW factors, corresponding to displacements spanning from $\sim 0.15 \text{ \AA}$, for the deeper layer, up to $\sim 0.45 \text{ \AA}$ for the topmost one. While a larger average displacement may be expected for a surface atom than for a bulk one, other mechanisms could be involved. In fact, large terraces are formed during LT layer-by-layer growth, which do not evolve after interruption of the evaporation. This implies a very high mobility of the Pb surface atoms, which contributes to the increase of the rms displacement.

The hierarchy of the layer depth is given both by the finite value of the X-ray penetration length for Pb (20 \AA), yielding different weights for different layers, and by the hierarchy of the DW factors (the smaller the deeper). As

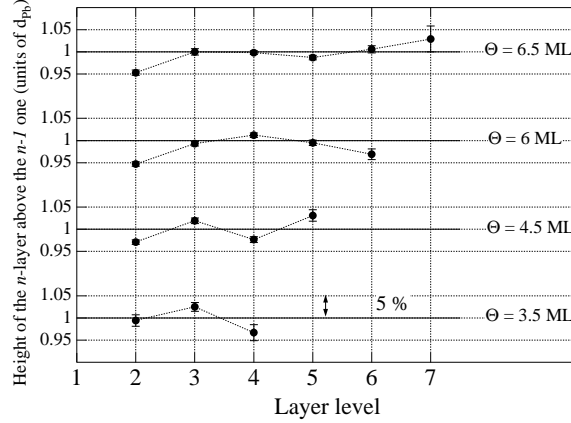


Fig. 11. Interlayer spacings in units of $d_{Pb(111)}$, as obtained by fitting to the rod scans of Fig. 10. For each film the height of the n -layer above the $(n - 1)$ -layer is given. The 1st layer distance from the interface cannot be determined since the simulation has been performed for a free-standing Pb(111) film.

can be seen from Fig. 11, the distance between the first (bottom) and second layer is always contracted up to $\sim 5\%$ of the bulk Pb(111) interlayer spacing. Given the free standing slab model used for the simulation, no information can be obtained about the height of the bottom layer of Pb(111) above the interface (whose thickness was also found by X-ray reflectivity to be contracted). More interestingly, it is clearly seen that the topmost layer height oscillates around the bulk value as new layers are added. In contrast to the calculations by Materzanini et al. [60], the atomic plane of the topmost layer is effectively following the surface charge density in its oscillatory behavior, yielding alternative expansion/compression of a few percent, as predicted by early calculations [37,38]. As expected [38], also the inner layer spacings display small relaxations (within 1-2 %). However, given the error bars and the increasing number of fitting parameters as the thickness increases, it is not possible to single out a general behavior for the inner layers. Only the subsurface layer seems to display an oscillating behavior (opposed to the oscillation of the topmost layer relaxation)

The absolute amount of the topmost layer relaxation is much lower than the amplitude of the apparent step height oscillation, as measured by HAS. In fact, a direct comparison between these two quantities is misleading, since the XRD analysis yields the height of a layer on top of another one, while HAS measures the apparent step height separating two adjacent terraces, i.e. two topmost layers of different height level. A more suitable term of comparison is the height difference between the XRD topmost layer of two consecutive thickness Pb films. The XRD step height is thus evaluated as $h_n^{XRD} = (d_n^{top} - d_{n-1}^{top}) + d_{Pb(111)}$ and shown in Fig. 12 in comparison with the HAS apparent step height. In this case the variation of the step height becomes relevant (exceeding $\pm 5\%$ of the bulk Pb(111) layer spacing), even if it is still lower than

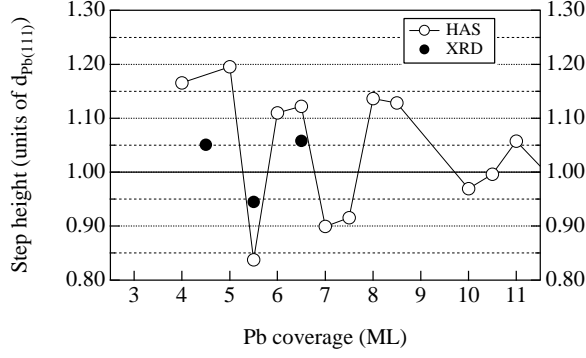


Fig. 12. The apparent step height obtained by direct HAS measurement is shown (open circles) together with the step height obtained by subtracting the XRD top-most layer spacings of consecutive film thickness (filled circles). The step height is given in units of $d_{Pb(111)}$.

the corresponding value obtained by HAS. Most importantly the step height oscillations effectively follow the surface charge density oscillations measured by HAS. The surface relaxation is thus strongly affected by QSE. A similar conclusion was indirectly obtained by the detailed STM spectroscopy study of Tsong and coworkers [40], who measured the oscillations of the apparent step height as a function of the tip bias voltage and found them to be present also for a reversed bias, thus indicating an effective structural variation of the step height.

4 Surface vibrations of thin Pb films

The variation of the surface relaxation due to QSE, although small, is sizeable and led us to study its influence on the Pb film vibrational properties by inelastic He scattering. If the variations of the topmost interlayer distance observed for different film thicknesses were large enough, they may be expected to alter also the force constants of the growing film and therefore modify the acoustic vibrations of the film. The phonon dispersion curves of the Pb(111) vibrational modes have been measured along the ΓM and ΓK (at 30° from ΓM) high symmetry directions within the 1st Brillouin zone (BZ) of the Pb(111) surface and compared for different Pb film thicknesses where the largest QSEs have been observed. The Time of Flight (TOF) spectra of low energy He atoms ($E_{He} = 19$ meV) have been acquired for different scattering geometries. All measurements have been performed at 130 K, where Pb thin films are stable enough to allow long time phonon data acquisitions. From the position of the inelastic peaks in the TOF spectra, the scattering events in which He atoms have exchanged energy and momentum quanta at the surface may be identified, i.e. scattering events in which surface phonons are created/annihilated. The resulting phonon dispersion obtained from over 20 TOF spectra taken at

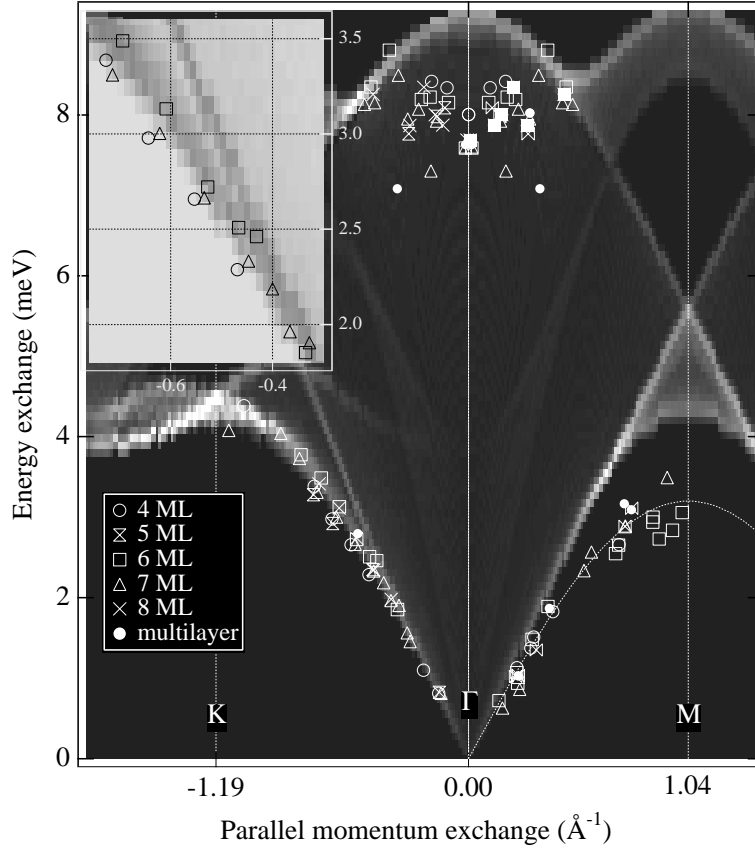


Fig. 13. The phonon spectra measured for a few thin Pb films of different thickness (open markers) and one thick film (filled marker) are shown in the first Surface Brillouin Zone (SBZ). The bulk vibrations, projected on the Pb(111) surface are also shown as shadowed bands, whose brightness is proportional to the corresponding cross-section for He inelastic scattering. In the inset (reversed gray scale), a small portion of the SBZ is enlarged to show the difference among phonon energies of 4, 6 and 7 ML Pb films.

different incidence angles is shown in Fig. 13. Since there are two 90° -rotated domains of Pb(111), both ΓM and ΓK phonon dispersion curves are detected along the same surface direction. Two distinct acoustic branches have been identified, one with a flat dispersionless behavior at 1.04 \AA^{-1} , corresponding to the Brillouin zone boundary along the ΓM surface direction and another one at higher frequencies, dispersing up to 1.19 \AA^{-1} (K point along the $\Gamma K M$ direction). Both branches have been identified a posteriori as acoustic branches along the ΓM and $\Gamma K M$ directions, respectively. This discrimination was not possible for high energy points appearing as an optical phonon branch close to the Γ point, thus they are reported along both ΓM and ΓK directions.

For comparison, Fig. 13 also shows the calculated vibrational spectra of an infinite Pb crystal projected on the (111) direction with Pb force constants

obtained from Ref. [66]. The shadowed area is obtained as the density of the bulk projected vibrational modes weighted with the component of the mode polarization along the surface normal in order to mimic the He inelastic cross section [67]. The experimental points along both ΓM and ΓK directions fall below the bulk projected area, confirming the surface character of the detected vibrational modes. An appreciable difference among the phonon energies of different films has been detected over a wide range of momentum exchange (see the inset panel in Fig. 13). For instance, along the ΓK surface direction, the observed phonon frequencies of the 6 ML Pb film are found to be higher than those of the 7 ML Pb film ($\sim 5\%$). However, a clear thickness dependent variation of the phonon frequencies could not be assigned. In fact, the effect of force constants variation due to topmost layer stretching/contraction is smeared or even cancelled out by the inner layer contraction/stretching.

5 Conclusions

Pb deposition on Ge(001) has been shown to proceed layer-by-layer when the substrate is held at temperatures lower than ~ 130 K. Similar findings have been found by a few authors for Pb deposited on Si(111) at even lower temperatures [21,22,23]. Such 2D heteroepitaxial growth may be expected from energy balance models when the Pb films exceed a critical thickness of five layers [34]. In fact, the occurrence of an initial transient regime, where Pb deposition proceeds by island growth, is commonly observed. The observed critical thickness seems to depend not only on the chemical nature of the substrate [28], but also on its temperature and terrace size. X-ray reflectivity appears to be the most reliable technique to measure the critical thickness, since it effectively probes the whole film. Both our XRR measurements and those for Pb/Si(111) [23] indicate the formation of a flat Pb surface after the deposition of 5 ML. At this thickness, a 2D growth is observed by both RHEED [22] and HAS [22,24] surface, yielding characteristic layer-by-layer oscillations. However, the transition from the island growth to the smooth growth might not be abrupt. In fact, our HAS data indicate that already at 4 ML a flat morphology is formed (see Fig. 2), but a complete wetting of the substrate is not met up to 5-6 ML. The complete wetting of the substrate could be driven by the mechanism envisaged for Ag deposited on Si(111) [25] and GaAs(110) [68], where a film with a flat surface of six layers is already formed at a coverage lower than 6 ML with several empty pits having steep perpendicular walls reaching the interface. Further Ag deposition leads to the formation of the next layers and pits filling.

For Pb on Ge(001), the LT growth could be described as follows. The first monolayer forms a pseudomorphic layer having almost the same atomic density of the close packed (111) plane [47], then Pb clusters are formed, which

soon display a Pb(111) crystal structure (in contrast to Pb on Si(111), where the crystal structure is formed at 5 ML). Flat Pb islands, probably interconnected, of homogeneous height level are formed at 4 ML, as witnessed by the appearance of the first maximum in HAS reflectivity. A complete substrate wetting is achieved at 6 M, and the corresponding film displays an extremely flat surface. Layer-by-layer growth is then observed up to a dozen of monolayers, with highly flat morphologies occurring at even-layer Pb coverage. At larger thickness, bi-layer modulations dominate the HAS reflectivity. The analysis of the XRD rod scans suggests that the Pb pseudomorphic layer is decomposed to contribute to the Pb(111) film. In fact, the number of Pb(111) layers within the film corresponds to the number of deposited Pb monolayers. On the contrary, the pseudomorphic layer produced by LT deposition on Si(111) has been found by XRD to be preserved also below a thick Pb film [62].

If the temperature is not low enough, or the substrate terrace size is not large enough, island growth sets in and the height correlation between different islands is lost, thus smearing the layer-by-layer features. For comparison, we recall that Pb islands are also observed for Pb deposition on Si(111) when the substrate temperature exceeds ~ 150 K [30,31,32], while layer-by-layer growth is achieved from 100 K [22] down to 16 K [21]. The 2D films grown on Ge(001) are metastable and their long range order can be increased by short annealing to ~ 190 K after LT Pb deposition. Upon annealing at higher temperature, the films are always irreversibly decomposed by fragmentation into uncorrelated 3D islands at any Pb film thickness. Metastability is also observed for Ag films on GaAs(110) at thickness higher than 6 ML. In this case the flat Ag islands formed by LT deposition are seen to coalesce into a flat wetting film upon annealing to room temperature [27]. Further annealing to 670 K irreversibly decomposes the Ag film into 3D mound-like islands.

The “electronic growth” model qualitatively describes the LT layer-by-layer growth of Pb on Ge(001), but a detailed calculation of the interface energetics would be needed to explain the observed larger stability of the even-layer Pb films (odd layer stability is predicted for Pb atoms [34]). An atomistic model of the diffusion and growth mechanism is still missing. The mechanism of funneling [69], proposed for the Pb/Si(111) system [21,22], does not seem to work in the present case (not exclusively, at least). In fact, the absence of surface diffusion would lead to a high island density, that, even if smoothed by the funnelling effect, would yield a large density of point defects, as a consequence the HAS reflectivity would be strongly reduced [70]. On the contrary the HAS reflectivity is extremely high (two order of magnitude higher than on the Ge(001) surface) and the Pb(111) domains display a mean size of several hundreds of Ångströms.

Quantum size effects have been observed to affect both the surface charge density and the surface relaxation of the growing Pb film. The strongest effect

is the apparent variation of the step height as measured by HAS [24]. In fact, the He turning point at the Pb(111) surface is displaced along the surface normal according to the in-vacuum decay of the electronic charge. Adjacent terraces of different height level display different decays of their surface charge density since they accommodate a different number of QWS [40]. The apparent step height, as measured by both HAS and STM, is thus affected since these investigation techniques are only sensitive to the surface charge density. The displacement of the charge density drives the displacement of the ionic cores, thus affecting the surface relaxation [37,38]. By XRD experiments, the extent of the structural QSE has been measured. Step height variations up to 5-6 % have been determined, as opposed to 20 % obtained by the HAS measurements. Although smaller than the displacement of the He turning point, the displacement of the topmost nuclear plane is non negligible, as previously thought [21,59,60]. Most importantly, the topmost layer effectively follows the direction of the charge density displacement, thus opening the way to the manifestation of other QSEs.

A sizeable variation of the surface relaxation may lead to the variation of the elastic force constant between the first and second topmost layers, thus affecting the acoustic vibrations. The dispersion of low energy surface phonons has been measured by inelastic HAS at different Pb film thickness. Appreciable differences among the phonon frequencies have been detected throughout the ΓK and ΓM direction of the first surface Brillouin zone. However, these differences could not be unambiguously correlated with the observed cyclic relaxations of the Pb topmost layer.

6 Acknowledgments

We are indebted with Fernando Tommasini who designed, realized and made working both the HAS apparatus and the ALOISA beamline. This project was partly funded by MURST cofin99 (Prot. 9902112831)

References

- [1] For a review on surface diffusion and growth see *Surface Diffusion, Atomistic and Collective Processes*, NATO ASI Series B, vol. 360, edited by M.C. Tringides, Plenum Press (New York, 1997).
- [2] S.Å. Lindgren and L. Walldén, in *Electronic Structure*, Handbook of Surface Science, vol. 2, chapt. 13, edited by K. Horn and M. Scheffler, Elsevier Science (Amsterdam, 2000).

- [3] T.C. Chiang, Surf. Sci. Rep. **39** (2000) 181.
- [4] M. Milun, P. Pervan and D.P. Woodruff, Rep. Prog. Phys. **65** (2002) 99.
- [5] P.D. Johnson, Rep. Prog. Phys. **60** (1997) 1217.
- [6] J.E. Ortega *et al.* Phys. Rev. B **47** (1993) 1540, J.E. Ortega and F.J. Himpsel, Phys. Rev. Lett. **69** (1992) 844.
- [7] M.D. Stiles, Phys. Rev. B **48** (1993) 7238.
- [8] P. Bruno, Phys. Rev. B **52** (1995) 411.
- [9] R.C. Jaklevic *et al.*, Phys. Rev. Lett. **26** (1971) 88; Phys. Rev. B **12** (1975) 4146.
- [10] S. ÅLindgren and L. Walldén, Phys. Rev. Lett. **59** (1987) 3003.
- [11] R.K. Kawakami, E. Rotenmberg, Hyuk J. Choi, Ernesto J. Escorcia-Aparicio, M.O. Bowen, J.H. Wolfe, E. Arhenolz, Z.D. Zhang, N.V. Smith, and Z.Q. Qiu, Nature (London) **398** (1999) 132.
- [12] J.J. Paggel, T. Miller, T.-C. Chiang, Science **283** (1999) 1709.
- [13] D.A. Evans, M. Alonso, R. Cimino and K. Horn, Phys. Rev. Lett. **70** (1993) 3483.
- [14] A. Arranz, J.F. Sánchez-Royo, V. Pérez-Dieste, P. Dumas and M.C. Asensio, Phys. Rev. B **65** (2002) 195410.
- [15] L. Aballe, C. Rogero and K. Horn, Phys. rev. B **65** (2002) 125319.
- [16] F.K. Schulte, Surf. Sci. **55**, 427 (1976).
- [17] $\lambda_F = 3.66 \text{ \AA}$ as evaluated from the Fermi energy of the bulk Pb, $E_F = 9.8 \text{ eV}$ and effective mass in the [111] direction of $m^* = 1.14m_0$, after Ref. [51]
- [18] M. Jalochowski and E. Bauer, Phys. Rev. B **38** (1988) 5272.
- [19] M. Jalochowski, E. Bauer, H. Knoppe and G. Lilienkamp, Phys. Rev. B **45** (1992) 13607.
- [20] M. Jalochowski, H. Knoppe, G. Lilienkamp and E. Bauer, Phys. Rev. B **46** (1992) 4693.
- [21] M. Jalochowski, M. Hoffmann, and E. Bauer, Phys. Rev. B **51** (1995) 7231.
- [22] D. Schmicker, T. Hibma, K.A. Edwards, P.B. Howes, J.E. MacDonald, M.A. James, M. Breeman, and G.T. Barkema, J. Phys. Condens. Matter **9** (1997) 969.
- [23] K.A. Edwards, P.B. Howes, J.E. MacDonald, T. Hibma, T. Bootsma, and M.A. James, Physica (Amsterdam) **221B** (1996) 201; Surf. Sci. **424** (1999) 169.
- [24] A. Crottini, D. Cvetko, L. Floreano, R. Gotter, A. Morgante, and F. Tommasini, Phys. Rev. Lett. **79** (1997) 1527.

- [25] L. Huang, S.J. Chey, and J.H. Weaver, Surf. Sci. Lett. **416** (1998) L1101.
- [26] A.R. Smith, K.-J. Chao, Q. Niu, and C.-K. Shih, Science **273** (1996) 226.
- [27] H. Yu, C.S. Jiang, Ph. Ebert, X.D. Wang, J.M. White, Q. Niu, Z. Zhang, and C.K. Shih, Phys. Rev. Lett. **88** (2002) 016102.
- [28] K.-J. Chao, Z. Zhang, Ph. Ebert, C.K. Shih, Phys. Rev. B **60** (1999) 4988.
- [29] L. Gavioli, K.R. Kimberlin, M.C. Tringides, J.F. Wendelken, and Z. Zhang, Phys. Rev. Lett. **82** (1999) 129.
- [30] K. Budde, E. Abram, V. Yeh, and M.C. Tringides, Phys. Rev. B **61** (2000) R10602.
- [31] M. Hupalo, V. Yeh, L. Berbil-Bautista, E. Abram, and M.C. Tringides, Phys. Rev. B **64** (2001) 155307.
- [32] M. Hupalo, S. Kremmer, V. Yeh, L. Berbil-Bautista, E. Abram, and M.C. Tringides, Surf. Sci. **493** (2001) 526.
- [33] V. Yeh, L. Berbil-Bautista, C.Z. Wang, K.M. Ho, and M.C. Tringides, Phys. Rev. Lett. **85** (2000) 5158.
- [34] Z. Zhang, Q. Niu, and C.-K. Shih, Phys. Rev. Lett. **80** (1998) 5381.
- [35] Z. Suo and Z. Zhang, Phys. Rev. B **58** (1998) 5116.
- [36] I.B. Altfeder, K.A. Matveev, and D.M. Chen, Phys. Rev. Lett. **78** (1997) 2815.
- [37] P.J. Feibelman, Phys. Rev. B **27** (1983) 1991 ; P.J. Feibelman, D.R. Hamann, Phys. Rev. B **29** (1984) 6463.
- [38] S. Ciraci and I.P. Batra, Phys. Rev. B **33** (1986) 4204; I.P. Batra, S. Ciraci, G.P. Srivastava, J.S. Nelson, and C.Y. Fong, Phys. Rev. B **34** (1986) 8246.
- [39] J.-H. Cho, Q. Niu, and Z. Zhang, Phys. Rev. Lett. **80** (1998) 3582; J.-H. Cho, Ismail, Z. Zhang, and E.W. Plummer, Phys. Rev. B **59** (1999) 1677.
- [40] W.B. Su, S.H. Chang, W.B. Jian, C.S. Chang, L.J. Chen, and Tien T. Tsong, Phys. Rev. Lett. **86** (2001) 5116.
- [41] D. Cvetko, A. Morgante, F. Tommasini, K. C. Prince and M. Sastry, Meas. Sci. Technol. **3** (1992) 997.
- [42] Details about the ALOISA end station can be found at the web address: "<http://tasc.area.trieste.it/tasc/lds/alois/aaloisa.html>".
- [43] D. Cvetko, L. Floreano, A. Crottini, A. Morgante, and F. Tommasini, Surf. Sci. Lett. **447** (2000) L147.
- [44] S. Ferrer, X. Torrelles, V.H. Etgens, H.A. van der Vegt, and P. Fajardo, Phys. Rev. Lett. **75** (1995) 1771.
- [45] C.S. Lent and P.I. Cohen, Surf. Sci. **139** (1984) 121.

- [46] W.S. Yang, X.-D. Wang, K. Cho, J. Kishimoto, T. Hashizume, and T. Sakurai, Phys. Rev. B **51** (1995) 7571; R.G. Zhao, Y. Zhang, and W.S. Yang, Phys. Rev. B **48** (1993) 8462; Y. Zhang, R.G. Zhao, and W.S. Yang, Surf. Sci. Lett. **293** (1993) L821.
- [47] O. Bunk, M.M. Nielsen, J.H. Zeysing, G. Falkenberg, F. Berg-Rasmussen, M. Nielsen, C. Kumpf, Y. Su, R. Feidenhans'l, R.L. Johnson, New J. Phys. **3** (2001) 13.1.
- [48] This mixed phase was erroneously identified with a (4×1) symmetry phase in Ref. [24].
- [49] It should be noted that the deposition curve published in Fig. 1 of Ref. [24] was not normalized to a constant deposition rate nor calibrated. In fact, the consecutive peak labelling of Ref. [24] is always referred to the deposition stages, which are easily identified with the corresponding ones shown in the present paper.
- [50] To be published elsewhere.
- [51] B.J. Hinch, C. Koziol, J.P. Toennies and G. Zhang, Europhys. Lett. **10** (1989) 341; Vacuum **42** (1991) 309.
- [52] H. Zeng and G. Vidali, Phys. Rev. Lett. **74** (1995) 582.
- [53] The Pb bulk lattice parameter is 4.95 \AA , and the distance between equivalent rows on the (111) surface is 3.03 \AA .
- [54] E. Weschke, C. Schüßler-Langeheine, R. Meier, G. Kaindl, C. Sutter, D. Abernathy, and G. Grübel, Phys. Rev. Lett. **79** (1997) 3954.
- [55] B.L. Henke, E.M. Gullikson, J.C. Davis, Atomic Data and Nuclear Data Tables **54** (1993) 181.
- [56] P.I. Cohen, G.S. Petrich, P.R. Pukite and G.J. Whaley, Surf. Sci. **216** (1989) 222.
- [57] H.A. van der Vegt, H.M. van Pinxteren, M. Lohmeier, E. Vlieg and J.M.C. Thornton, Phys. Rev. Lett. **68** (1992) 3335.
- [58] Layer-by-layer erosion, can be obtained by low energy Ar^+ ion bombardment also on semiconductors. As an example see: D. Cvetko, V. De Renzi, L. Floreano, A. Morgante, M. Peloi, F. Tommasini, V. Chab and K.C. Prince, Phys. Rev. B **51** (1995) 17957.
- [59] J. Braun and J.P. Toennies, Surf. Sci. **384** (1997) L858.
- [60] G. Materzanini, P. Saalfrank, and P.J.D. Lindan, Phys. Rev. B **63** (2001) 235405.
- [61] Y.S. Li, F. Jona, and P.M. Marcus, Phys. Rev. B **43** (1991) 6337.
- [62] P.B. Howes, K.A. Edwards, D.J. Hughes, J.E. MacDonald, T. Hibma, M.A. James, and T. Bootsma, Phys. Rev. B **51** (1995) 17740.

- [63] F. Bruno, *Methods for growth experiments at ALOISA*, PhD Thesis, University of Trieste, (2001) Trieste.
- [64] E. Vlieg, J. Appl. Cryst. **33** (2000) 401.
- [65] L.-M. Pend, G. Ren, S.L. Dudarev and M.J. Whelan, Acta Cryst. **A52** (1996) 456.
- [66] Landolt-Börnstein, Condensed Matter **110** (Springer-Verlag, Berlin, 1999).
- [67] in our geometry, inelastic scattering has the largest cross-section for surface phonons with a polarization normal to the surface. See for example: M. Buongiorno Nardelli, D. Cvetko, V. De Renzi, L. Floreano, A. Morgante, M. Peloi, and F. Tommasini, Phys. Rev. B **52** (1995) 16720.
- [68] M.M.R. Evans, B.Y. Han, and J.H. Weaver, Surf. Sci. **465** (2000) 90.
- [69] J.W. Evans, D.E. Sanders, P.A. Thiel, and A.E. DePristo, Phys. Rev. B **41** (1990) 5410.
- [70] Point-like and linear defects give rise to incoherent scattering over the whole solid angle, causing a net intensity decrease in the specular direction. The cross section for He scattering from single adatoms or vacancies on metal surfaces is typically 100–150 Å². See: B. Poelsema, K. Lenz, L.S. Brown, L.K. Verheij, and G. Comsa, Surf. Sci. **162** (1985) 1011.